

# CFD Simulation of Effect of Interphase Forces and Turbulence Models on Gas–Liquid Two-Phase Flows in Non-Industrial Aluminum Electrolysis Cells

SHUIQING ZHAN,<sup>1</sup> JIANHONG YANG,<sup>2,4</sup> ZHENTAO WANG,<sup>1</sup>  
RUIJIE ZHAO,<sup>3</sup> JUN ZHENG,<sup>1</sup> and JUNFENG WANG<sup>1</sup>

1.—School of Energy and Power Engineering, Jiangsu University, Zhenjiang 212013, People's Republic of China. 2.—School of Material Science & Engineering, Jiangsu University, Zhenjiang 212013, People's Republic of China. 3.—Research Center of Fluid Machinery Engineering and Technology, Jiangsu University, Zhenjiang 212013, People's Republic of China. 4.—e-mail: jhyang\_qx@yahoo.com

Numerical simulations of gas–liquid two-phase flows in aluminum electrolysis cells using the Euler–Euler approach were presented. The attempt was made to assess the performance and applicability of different interphase forces (drag, lift, wall lubrication, and turbulent dispersion forces) and turbulence models (standard  $k$ – $\epsilon$ , renormalization group  $k$ – $\epsilon$ , standard  $k$ – $\omega$ , shear stress transport  $k$ – $\omega$ , and Reynolds stress models). Moreover, three different bubble-induced turbulence models have been also analyzed. The simulated electrolyte velocity profiles were discussed by comparing with each other and against published experimental data. Based on the results of the validation of different interphase forces and turbulence models, a set consisting of the dispersed standard  $k$ – $\epsilon$  model, Grace drag coefficient model, Simonin turbulent dispersion force model, and Sato et al.'s bubble-induced effective viscosity model was found to provide the best agreement with the experimental data. The prediction results showed that the contributions of the lift force and the wall lubrication force can be neglected for the present bubbly flows.

## INTRODUCTION

During the operation of commercial aluminum electrolysis cells, the anode gases are mainly generated under the anode bottom surfaces and move up through the molten electrolyte with the recirculation flows. The performance of gas-induced electrolyte flows has a significant impact on the homogenization of alumina concentration, cell design, and energy saving.<sup>1</sup> Therefore, the development of gas–liquid two-phase flows is essential to deeply understand the complex flow behavior and the efficient design and scale-up of electrolysis reactors.

Over the past few decades, both experimental and simulation methods have been extensively used for aluminum electrolysis. The experimental methods mainly based on laboratory cells and physical models have been reviewed by Cooksey et al.<sup>2</sup> These investigations were mainly focused on obtaining

single bubble dynamic behaviors and remain somewhat limited to qualitative analysis. To date, with the rapid advancements in computational fluid dynamics (CFD) methods, many CFD studies have been performed to predict the gas–liquid flows in cells. Specifically, the two-fluid model based on the classic Euler–Euler methodology is favored and most widely used because of its lower computational resources.<sup>3–5</sup> There is no doubt that the correct CFD modeling of interphase forces and turbulence models is of great importance for capturing the gas–liquid flows properly.

The interphase forces (drag and non-drag forces) play a very important role in the interphase momentum transport between phases. Several widely used interphase force models are available in the literature for different bubbly flows. Nevertheless, it is generally agreed that the drag force is predominant over other non-drag forces, such as the lift, virtual mass, wall lubrication, and turbulent

dispersion forces.<sup>6</sup> Therefore, researchers in most studies have only considered the drag force for modeling of gas–liquid flows in aluminum electrolysis cells.<sup>3,5,7,8</sup> So far, only Feng et al.<sup>4,9</sup> have taken into consideration the drag and turbulent dispersion forces together in CFD simulations. Moreover, two different drag force models, namely Ishii and Zuber<sup>10</sup> and Schiller and Naumann,<sup>11</sup> were used by the researchers in the two aforementioned studies, respectively. Although these investigations have yielded reasonable results, no work has so far included the collective effects of more interphase forces together on the gas–liquid flows. CFD simulations of the effects of different interphase force models have limitations as a result of the complex hydrodynamics, and the lack of reliable experimental data for verification and validation. Some limited attempts only relied on experience, and there are no more comprehensive reports about the influence mechanism of the interphase forces in cells.

Besides these interphase forces, the turbulence model has also received considerable attention. Different turbulence models have been employed for two-phase bubbly systems.<sup>12</sup> For the gas–liquid flows in cells, the widely used standard  $k$ – $\varepsilon$  model was applied by the researchers in all previously studies reported.<sup>4,5,7–9</sup> Although such an approach is highly desirable, the physical mechanisms are still not fully understood. Moreover, it is generally considered that the turbulence mainly includes the bulk turbulent effect and the bubble-induced turbulence (BIT). Two different approaches, such as a bubble-induced contribution to the effective viscosity and bubble-induced source terms, have been widely employed for the bubbly flows.<sup>13</sup> Most investigations have incorporated an additional contribution to the turbulent viscosity of Sato et al.<sup>14</sup> to account for the BIT in cells.<sup>4,5,7–9</sup> Feng et al.<sup>4,9</sup> studied the effects of two different BIT methods and showed that the BIT models with source terms gave a better qualitative prediction than Sato et al.’s model.<sup>14</sup> Nevertheless, there is so far no general evaluation for such issue with limited unknown information in different operational cells.

In this work, an attempt has been first made to study the effects of different interphase forces (drag, lift, wall lubrication, and turbulent dispersion forces) on the gas–liquid flows in aluminum electrolysis cells. Afterward, the comparative performance of different turbulence models (standard  $k$ – $\varepsilon$ , RNG  $k$ – $\varepsilon$ , standard  $k$ – $\omega$ , SST  $k$ – $\omega$ , and RSM models) are presented. Furthermore, the applicability of three different BIT models is investigated in detail. The simulated results are compared with each other and against experimental data of Cooksey and Yang.<sup>15</sup> It should be underlined that, to the authors’ knowledge, this work is the first in which such comparison is made.

## MATHEMATICAL MODEL

### Two-Fluid Model

The mathematical model is formulated based on the Euler–Euler two-fluid model, in which both the continuous (electrolyte) and dispersed (gas) phases are considered to be interpenetrating continuous media. The continuity and momentum balance equations can be written as:

$$\frac{\partial}{\partial t}(\rho_q \alpha_q) + \nabla \cdot (\rho_q \alpha_q \mathbf{u}_q) = 0 \quad (1)$$

$$\begin{aligned} & \frac{\partial(\alpha_q \rho_q \mathbf{u}_q)}{\partial t} + \nabla \cdot (\alpha_q \rho_q \mathbf{u}_q \mathbf{u}_q) \\ & = -\alpha_q \nabla P + \nabla \cdot \left( \alpha_q \mu_{\text{eff},q} \left( \nabla \mathbf{u}_q + (\nabla \mathbf{u}_q)^T \right) \right) \\ & \quad + \alpha_q \rho_q \mathbf{g} + \mathbf{F}_q \end{aligned} \quad (2)$$

where  $\alpha_q$ ,  $\rho_q$ ,  $\mathbf{u}_q$  are the volume fraction, density, and velocity of the phase  $q$  ( $l$  for liquid and  $g$  for gas), respectively.  $\mu_{\text{eff},q}$  is the effective viscosity of phase  $q$ ,  $P$  is the pressure, and  $\mathbf{g}$  is the gravity constant.  $\mathbf{F}_q$  stands for the interphase forces.

### Interphase Force Model

The total interphase forces include the drag force ( $\mathbf{F}_D$ ), lift force ( $\mathbf{F}_L$ ), wall lubrication force ( $\mathbf{F}_{\text{WL}}$ ), and turbulent dispersion force ( $\mathbf{F}_{\text{TD}}$ ). The virtual mass force ( $\mathbf{F}_{\text{VM}}$ ) has been neglected throughout this paper as the steady state of electrolyte flow is concerned for the present study:

$$\mathbf{F}_q = \mathbf{F}_D + \mathbf{F}_L + \mathbf{F}_{\text{WL}} + \mathbf{F}_{\text{TD}} \quad (3)$$

The drag force opposes to the motion of bubbly within fluids and proportional to the slip velocity between the gas and liquid phases, which can be formulated as:

$$\mathbf{F}_D = \frac{3}{4} \frac{C_D}{d_b} \alpha_g \alpha_l \rho_l |\mathbf{u}_l - \mathbf{u}_g| (\mathbf{u}_l - \mathbf{u}_g) \quad (4)$$

where  $C_D$  is the drag coefficient taking into account the character of the liquid flow around the individual bubbles.  $d_b$  is the mean bubble diameter, which equals 7.0 mm in the current study.

Given the lack of information about the drag force affecting both phases and complex bubbly flow regimes in the real cells, various drag coefficient models are employed and compared in Table SI in the supplemental material.

The lift force mainly arises from the vortex effect and the horizontal velocity gradients in shear flow. This force in terms of the relative velocity and the curl of the liquid phase velocity can be described as:

$$\mathbf{F}_L = -C_L \alpha_g \rho_l (\mathbf{u}_l - \mathbf{u}_g) \times (\nabla \times \mathbf{u}_l) \quad (5)$$

where  $C_L$  is the lift coefficient.

Under certain circumstances, the dispersed bubble is observed to concentrate in a region close to the wall but not immediately adjacent to the wall. This effect may be modeled by the wall lubrication force with a general form as:

$$F_{\text{WL}} = -C_{\text{WL}}\alpha_g\rho_l\left|\left(\mathbf{u}_l - \mathbf{u}_g\right)\right|_{\parallel}^2\vec{n}_w \quad (6)$$

where  $C_{\text{WL}}$  is the wall lubrication coefficient.

The turbulent dispersion force accounts for the turbulent fluctuation of liquid velocity and the effect on the bubbles. This force is derived by the ensemble average of the fluctuating component of the drag forces between the bubbles and liquid phase. In this work, various available turbulent dispersion force correlations ( $C_{\text{TD}} = 0.2$ ) used in most of the gas–liquid bubbly flows and other interphase force models<sup>16</sup> are synthesized and compared in Table SI in the supplemental material.

### Turbulence Model

The turbulence model determines the turbulent structure in two-phase flows. As a result of the existence of bubbles, the turbulence becomes more complex, and thus, no standard turbulence model is applicable for different gas–liquid flows. Three turbulence models of the  $k-\varepsilon$ ,  $k-\omega$ , and RSM are considered in this work. Furthermore, ANSYS Fluent provides three different secondary phase considerations for modeling turbulence in multiphase flow. In terms of aluminum electrolysis simulation, the density ratio between the two phases is larger than 5000 and the main flow regions under the anode bottom surfaces contain one continuous phase (electrolyte) and a dilute secondary phase in the form of bubbles. Therefore, the dispersed turbulence model is the most appropriate model. For this reason, only the dispersed turbulence model was investigated in this study. As a result of the constraints on the length of this article, the detailed equations and the physical characteristics will not be repeated here, but they can be found in ANSYS Fluent 14.5.<sup>16</sup>

For gas–liquid flows, the dispersed bubbles affect the liquid turbulence. Development of a suitable model for BIT mentioned earlier, therefore, is a key element in getting complete and predictive CFD simulations. Various models are available for accounting for the turbulence induced by the bubbles' movement. Adding an extra bubble-induced term for modifying effective viscosity and adding a source of bubble-induced turbulent energy are the most widely used methods. A detailed derivation of the additional contribution to the turbulent viscosity of Sato et al.<sup>14</sup> can be found in our previous work.<sup>17</sup> Moreover, two different bubble-induced source terms that can be added directly to the generation terms in the turbulence equations are shown in Table SII in the supplemental material.

### NUMERICAL DETAILS

The CFD simulations of gas–liquid two-phase flows have been validated with experimental data using the particle image velocimetry (PIV) taken on the air–water model described by Cooksey and Yang.<sup>15</sup> The geometry setup and the structural hexahedra grinding are shown in Fig. S1 in the supplemental material. Using the same conditions as the experiments, the anode–cathode distance was 0.04 m. The widths of the interanode, side, center, Tap-end, and Duct-end channels were 0.04 m, 0.24 m, 0.12 m, 0.16 m, and 0.04 m, respectively. The PIV measurements were mainly conducted and validated at three different vertical planes and locations ( $z=0.08$  m,  $z=0.12$  m, and  $z=0.16$  m) as shown in Fig. S1b. In addition, more details of the quantitative comparison for several traverses at different heights and locations (Locations A, B, C and D, see work of Cooksey and Yang<sup>15</sup>) on the air–water model for all various submodels have been added in the work. Since the bubble behavior was very complicated and important in the ACDs and the interanode channels than in other flow regions, a local grid refinement approach was presented as shown in Fig. S1d and e. The grid independence results will be provided in the next sections.

The CFD simulations were conducted on the ANSYS Fluent 14.5 platform. A mass-flow-inlet boundary condition was applied under the anode bottom surfaces. The mass flow rate of anode gas generation was obtained by the well-known Faraday laws of electrolysis. On the top surface of the electrolyte, a degassing boundary condition was applied. No-slip and free-slip boundary conditions were applied for the liquid and gas bubbles at the wall. The density and viscosity of the electrolyte was taken at  $2130$  kg/m<sup>3</sup> and  $2.51 \times 10^{-3}$  Pa s, whereas those for the gas were at  $0.398$  kg/m<sup>3</sup> and  $5.05 \times 10^{-5}$  Pa s, respectively.

### RESULTS AND DISCUSSION

All test cases were simulated with the interphase forces and turbulence models as described in the previous sections. Based on the previous experience, the following set of models (dispersed standard  $k-\varepsilon$  model, Grace drag coefficient model, Simonin turbulent dispersion force model, and Sato et al.'s bubble-induced effective viscosity model) were selected as the basis to perform the differential analysis. The simulations were carried out by changing the different models of interest while keeping the other models unchanged. A detailed comparison is made between the simulated and measured vertical electrolyte velocity profiles in the side channel.

#### Grid Independence Study

Before the formal simulations, the grid independence tests were conducted among different grid cells of 43,376 (Grid1), 84,150 (Grid2), 165,415

(Grid3), 311,070 (Grid4), and 645,274 (Grid5). In the grid dependency evaluation, the tests were performed with a Schiller–Naumann drag coefficient model.

The predicted gas volume fraction distributions at a horizontal plane ( $z = 0.03$  m) were compared as shown in Fig. S2 in the supplemental material. It can be seen that the gas distribution patterns almost do not change when the grid cells increase beyond 165,415 (Grid3). For a quantified validation, the simulated vertical electrolyte velocity distributions with different grid resolutions were extracted and compared with the experimental data, as shown in Fig. S3. It can be seen that in the grid cells from 311,070 (Grid4), there is practically no change in the results presented for the finer grids. Therefore, the Grid4 will be chosen for all the subsequent simulations. It should be noted that there is still a larger deviation between the predicted and experimental results for the finer grids, although the modeling with grid independence has achieved good effects. For a more appropriate comparison, improved models need to be conducted in the following several sections.

### Effect of Drag Force Model

In the present work, the predicted results for different drag coefficient models of Schiller–Naumann, Ishii–Zuber,  $C_D = 0.44$ , Tomiyama, and Grace were tested and compared, as shown in Fig. 1. It can be clearly seen that the agreement with the experimental data is improved significantly with the drag coefficient models of Ishii–Zuber, Tomiyama, and Grace compared with that of Schiller–Naumann and  $C_D = 0.44$  (Fig. 1a, b, and c). But at the traverses of  $z = -0.16$  m and  $z = -0.12$  m in Location C, the models of Schiller–Naumann and  $C_D = 0.44$  give better agreement with the experimental results. Also, the results with the first three drag coefficient models have changed significantly. The better prediction by the first three models can be attributed to the drag coefficient being a function of the bubble Reynolds number instead of a constant value when the bubble Reynolds number exceeds 1000. Furthermore, these three models can produce higher drag coefficients because they are formulated based on the data of individual bubbles with complex flow regimes. In view of this, it can lower the slip velocity, drive more bubbles, and generally increase higher electrolyte velocity. This is not unexpected because the gas volume fraction under the anode bottom surfaces is very high,<sup>17</sup> and hence, the system may produce bubbles with different diameters, shapes, regimes (spherical, hemispherical, and spherical cap), and velocities. Therefore, the Schiller–Naumann model cannot be safely used in the simulations. Moreover, it was observed that the Grace drag coefficient model gave better prediction

than both the Ishii–Zuber and Tomiyama models in the whole regions. Hence, the Grace drag coefficient model was chosen for further closure verification.

### Effect of Lift Force Model

The effects of different lift coefficients models were investigated, and the predicted results are shown in Fig. 2. It is obvious that using the lift force has no significant effect on the CFD results in comparison with the case without considering the lift force. This means that the transverse force caused by lateral movement of bubbles can be neglected in the side channels. Moreover, it was found that the convergence is much harder to reach when the lift force was considered. Therefore, the lift force was not recommended in the next study. For sure, the predicted electrolyte velocities for all other comparisons are generally similar to the present results (Fig. 2), which can be not given here.

### Effect of Wall Lubrication Force Model

The three widely used wall lubrication coefficient models, including Antal, Tomiyama, and Frank, were considered. The predicted results with and without consideration of the wall lubrication force were compared as shown in Fig. 3. Compared with the experimental data, the case with the wall lubrication force is nearly the same as the case without considering the wall lubrication force. Furthermore, even with the use of the different models, the predicted result has hardly changed. This is because the bubbles are mainly distributed under the regions of the anode bottom surfaces (see Fig. S2 in the supplemental material). The effect of the wall lubrication force was negligible for the small gas volume fractions in the regions near the anode walls, which has been discussed in our previous work.<sup>17</sup> From these simulations, the wall lubrication force was negligible in the rest of the work. For the same reasons as the case of the effect of lift force model, the predicted results for all other comparisons are not given here.

### Effect of Turbulent Dispersion Models

Simulations were carried out for three different turbulent dispersion force models, and the predicted results are shown in Fig. 4. The turbulent dispersion force shows some effects on the simulated results. The Simonin model shows better results with the experimental data than with the models of Lopez-de-Bertodano and Burns, especially for the regions near the cell walls. Nevertheless, when the Burns model was used, there was a small negative influence on the results compared with the case without considering the turbulent dispersion force. As stated earlier, the turbulent dispersion force models were correlated with the turbulent parameters in the two-phase flows, such as the turbulent

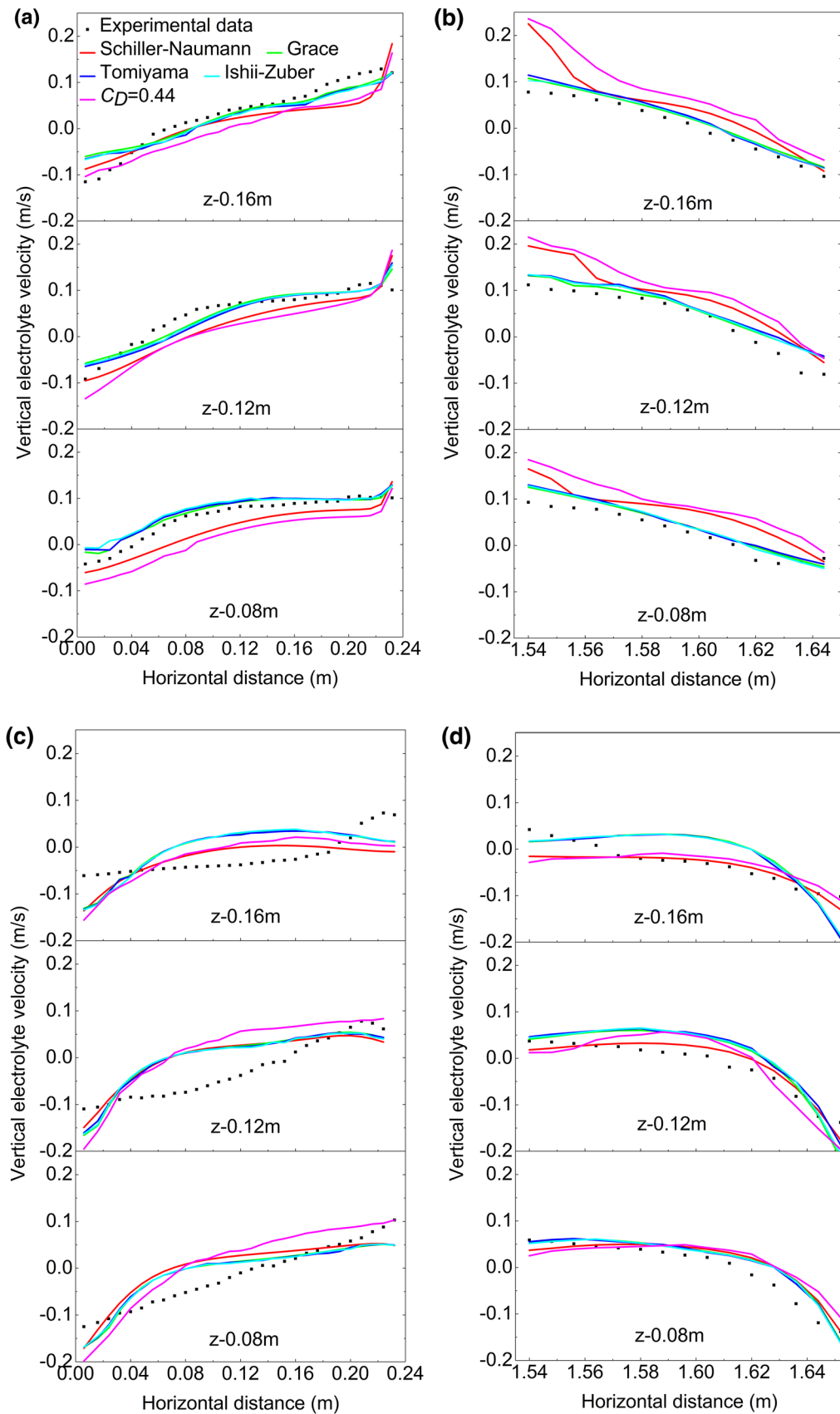


Fig. 1. Comparisons of vertical electrolyte velocity profiles for different drag coefficient models: (a) Location A, (b) Location B, (c) Location C, and (d) Location D.

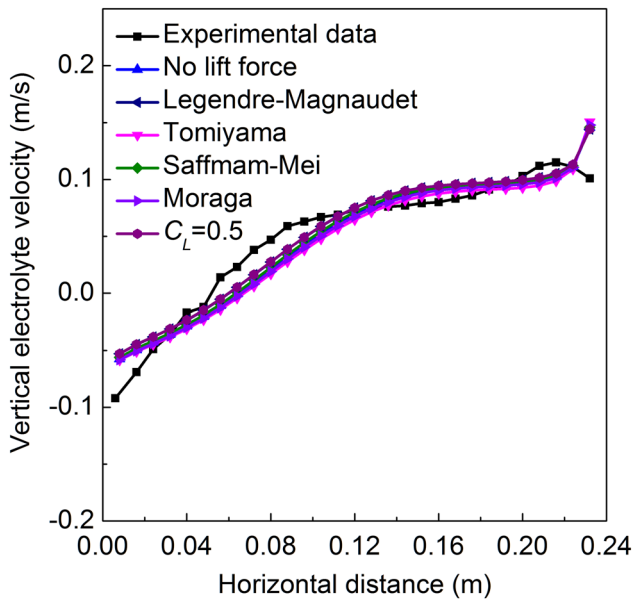


Fig. 2. Comparisons of vertical electrolyte velocity profiles for different lift coefficient models.

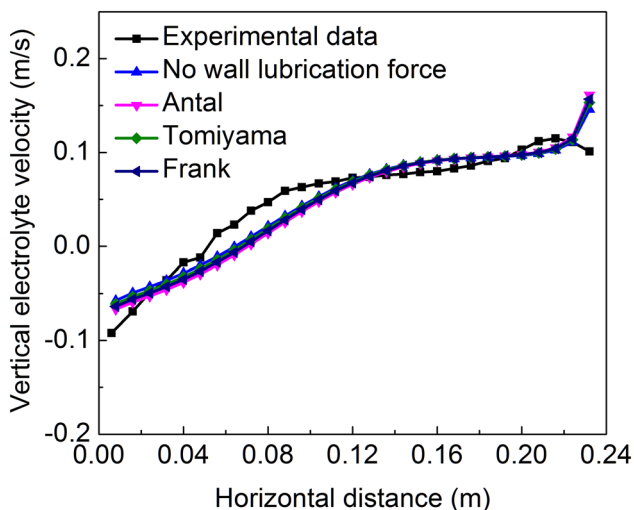


Fig. 3. Comparisons of vertical electrolyte velocity profiles for different wall lubrication force models.

viscosity and the turbulent kinetic energy. Therefore, the rational use of this force is an important part of the current work and the Simonin turbulent dispersion force model will be used for further research.

### Effect of Turbulence Model

In addition to the effects of the interphase forces, the proper turbulence description is one of the critical points in capturing the hydrodynamic properties of the aluminum electrolysis cells. Thus, an analysis and comparison for different dispersed

turbulence models, including the  $k-\varepsilon$  model,  $k-\omega$  model, and the RSM model, were also performed in this study.

Figure 5 shows the effects of five different dispersed turbulence models on the predicted vertical electrolyte velocity distributions. As can be seen by comparing, excluding the dispersed RSM model, the turbulence models investigated have a similar influence on the vertical electrolyte velocity distributions. The predicted electrolyte velocities of the dispersed RSM model change significantly in comparison with the experimental data (see Fig. 5b and d), and the predicted vertical electrolyte velocity distribution is different than that predicted by the other models. With careful visual inspection, it can be observed that the dispersed standard  $k-\varepsilon$  model gives the best prediction with the experimental data. From the previous discussion, it can be concluded that the dispersed standard  $k-\varepsilon$  turbulence model is appropriate for the simulation of hydrodynamic in aluminum electrolysis cells and that this model requires less computation than other models.

### Effect of BIT Model

The effects of three different BIT models on the CFD results were given as shown in Fig. 6. From the local influence analysis of view, it is clear that the electrolyte velocity profiles show the positive impact of the BIT models at the regions near the cell walls, but some small negative influence can also be found at the regions near the anode walls. The overall deviation between the simulated results obtained by Sato et al.'s model and the experimental data is smaller than the cases with the other two BIT models and the case without the BIT model. The Troshko-Hassan model performed worse than the Simonin model did over the whole region. In Sato et al.'s model, an analytical relationship was derived for evaluating the additional turbulence; thus, a good relationship has been built theoretically by such a treatment between the liquid velocity and the gas volume fraction. The predicted results indicated that the inclusion of Sato et al.'s bubble-induced effective viscosity model is necessary to model aluminum electrolysis behavior correctly.

### Verification of Selected Models

Based on the previous analysis, a verification strategy for the selected models (dispersed standard  $k-\varepsilon$  model, Grace drag coefficient model, Simonin turbulent dispersion force model, and Sato et al.'s bubble-induced effective viscosity model) was proposed. The predicted global flow patterns are generally similar to the PIV experimental results, which can be seen in our previous work<sup>18-20</sup> and are not given here. The quantitative comparisons between the PIV experimental and predicted results for several traverses at different heights and

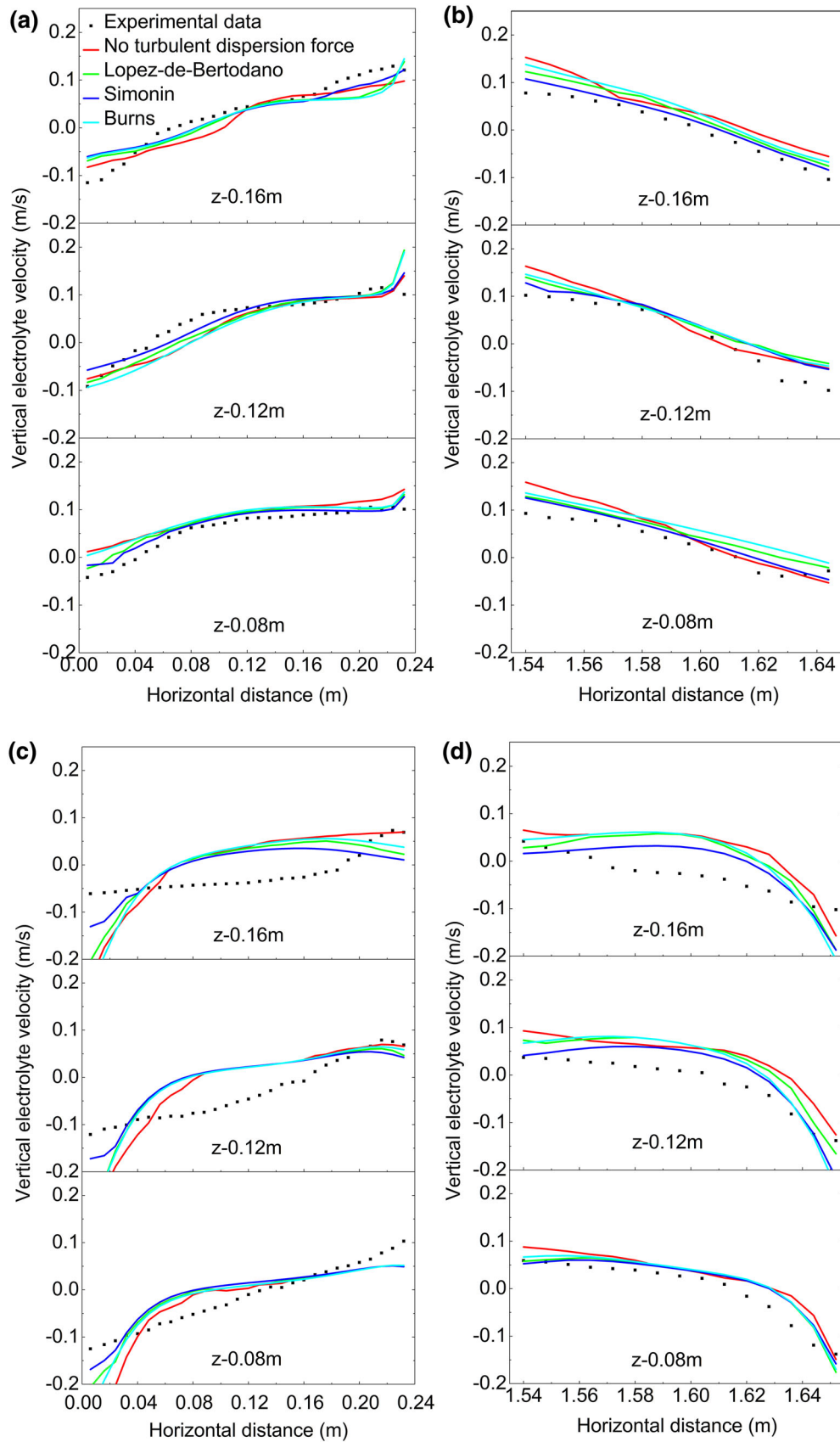


Fig. 4. Comparisons of vertical electrolyte velocity profiles for different turbulent dispersion force models: (a) Location A, (b) Location B, (c) Location C, and (d) Location D.

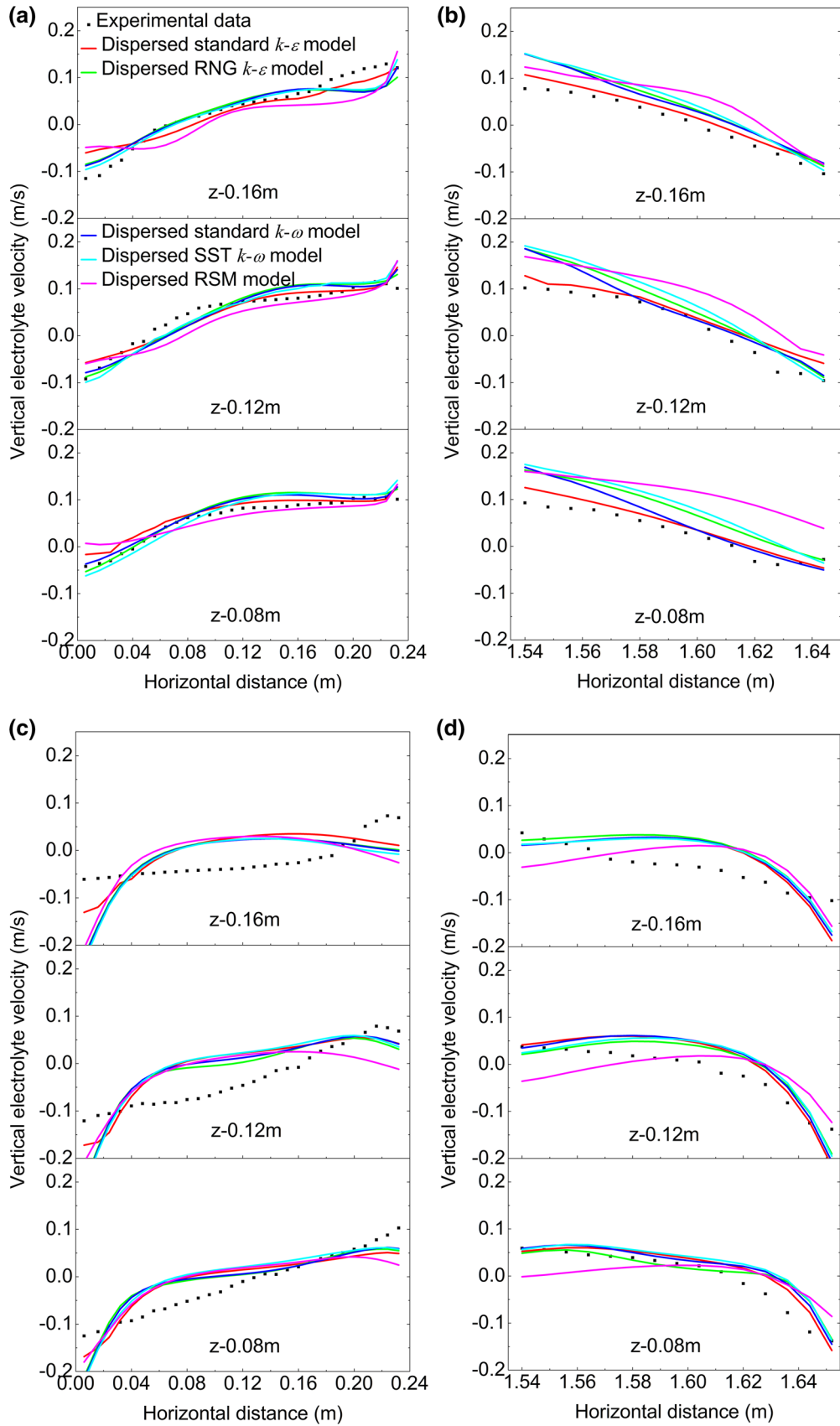


Fig. 5. Comparisons of vertical electrolyte velocity profiles for different dispersed turbulence models: (a) Location A, (b) Location B, (c) Location C, and (d) Location D.



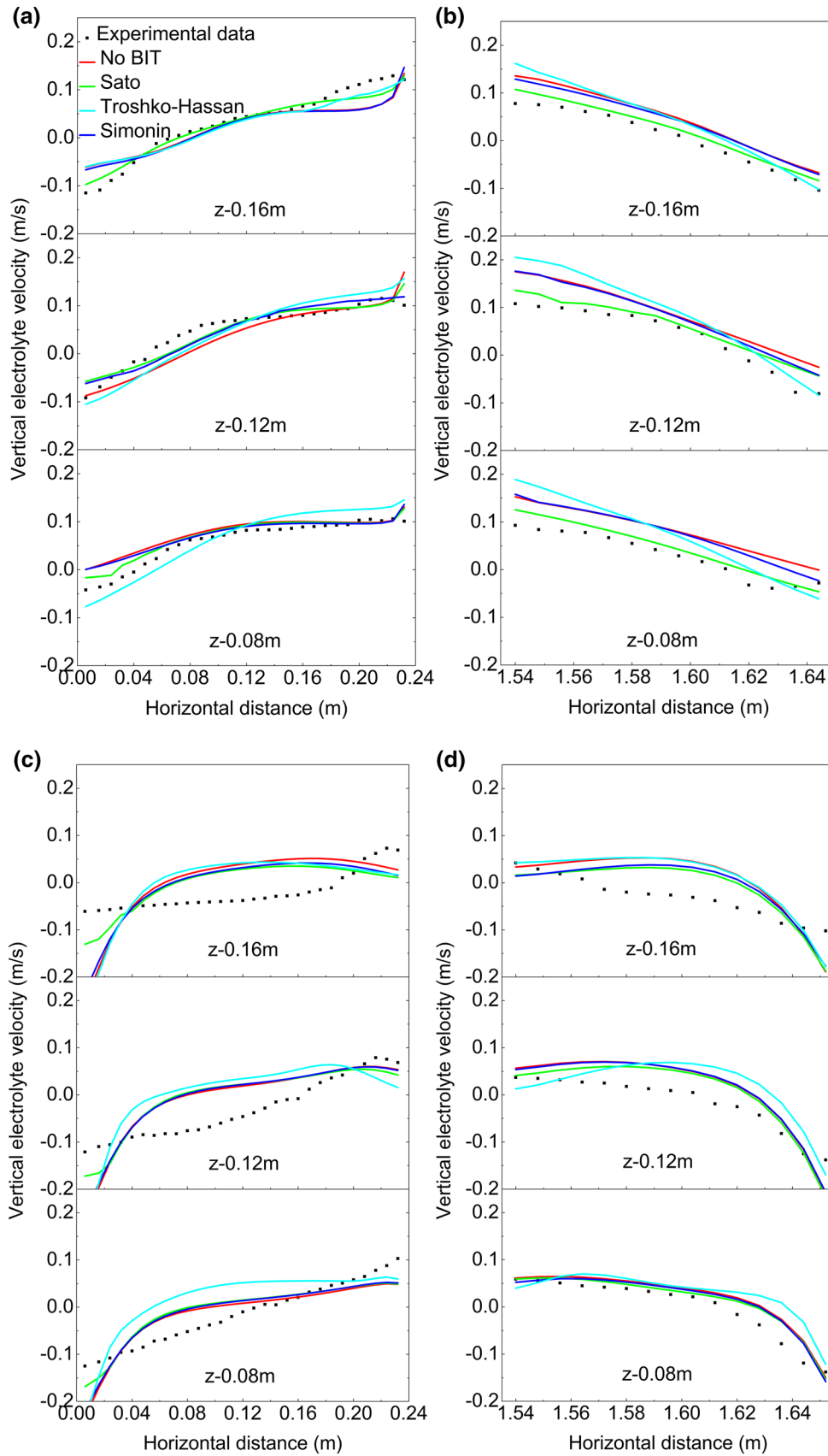


Fig. 6. Comparisons of vertical electrolyte velocity profiles for different BIT models: (a) Location A, (b) Location B, (c) Location C, and (d) Location D.

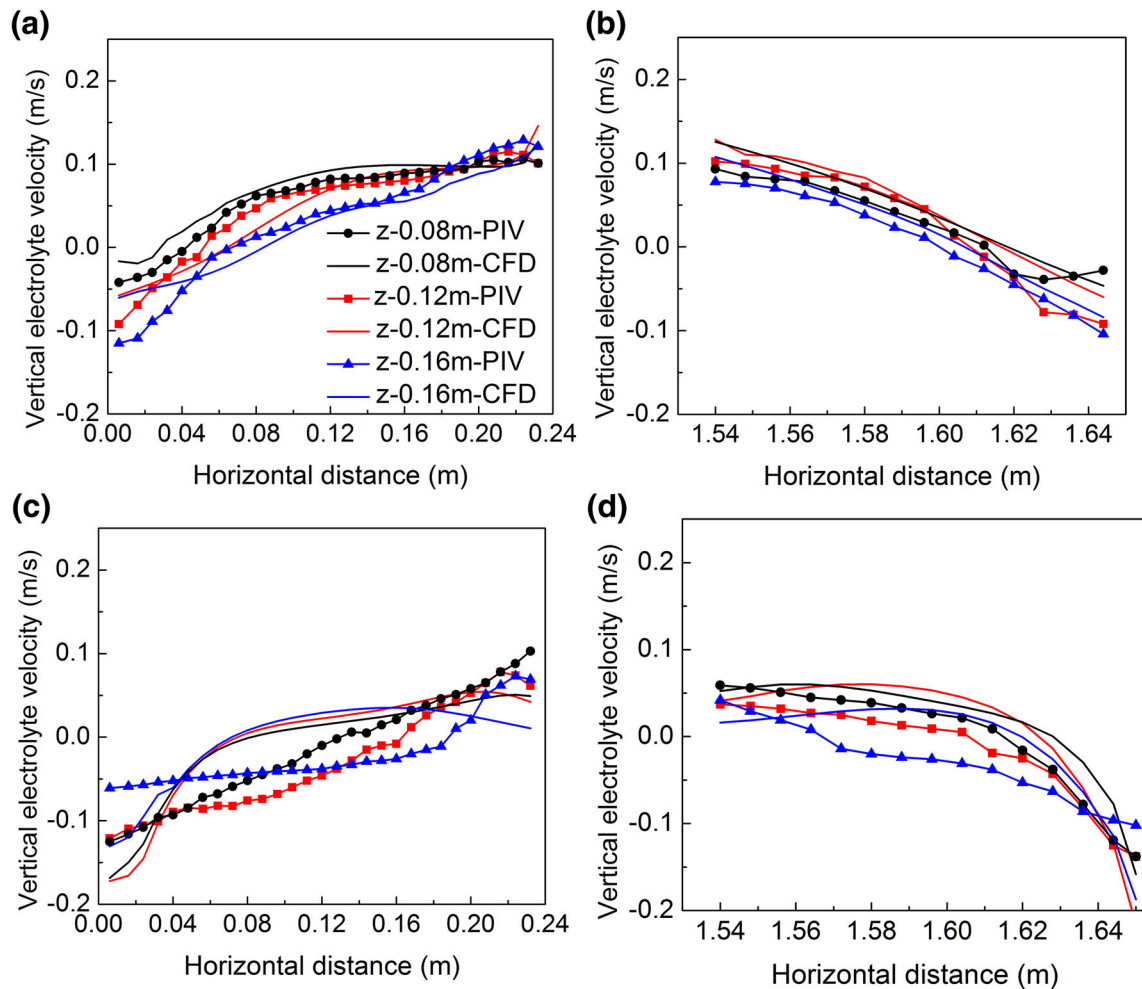


Fig. 7. Comparisons of vertical electrolyte profiles for different traverses at different heights and locations: (a) Location A, (b) Location B, (c) Location C, and (d) Location D.

locations are shown in Fig. 7. The detailed locations and flows information can be found in Ref. 15. It can be seen that good agreement has been obtained in most regions for the transverse plane through the middle of the middle anode (Fig. 7a and b). At the same time, the agreement is generally not so good between the experimental and predicted velocities on the plane through the middle of the interanode gap (Fig. 7c and d). These obvious differences mainly show in the middle regions of both the side and center channels, respectively, where the upward water velocity is overestimated. The predicted results at both heights of 0.12 m and 0.16 m show that these flow field characteristics are more obvious. This is mainly because the upward flow plume reinforces the recirculation along both the entire length of the two channels and introduces some water movement along the length of the channels away from the interanode gap. The conclusion drawn is consistent with the results reported previously by Feng.<sup>9</sup> For this situation,

the further modification and optimization should be made based on the detailed flow patterns and on the analyzed characteristics of each selected model indicated in the former step.

## CONCLUSION

CFD simulations have been performed to study the effects of different interphase forces and different turbulence models on the gas–liquid two-phase flows in aluminum electrolysis cells. In addition, the effects of different BIT methods were also investigated. Following are the conclusions.

The significance of appropriate selection of drag coefficient models has been presented. It was found that the closure model for the drag force strongly affects the vertical electrolyte velocity distributions. The Grace drag coefficient model provides a better solution when compared with all other drag force correlations. The lift and wall lubrication forces on the electrolyte flows are both found to be

insignificant and can be neglected in the current model. The turbulent dispersion force shows a certain effect on the results, and the Somonin turbulent dispersion force model shows better results when compared with the other formulations.

The prediction of the dispersed standard  $k$ – $\epsilon$  model shows better agreement with the experimental data as compared with the other turbulence formulations. The BIT models have a significant influence on the gas–liquid flows. The approach using Sato et al.'s bubble-induced effective viscosity model gives better results with the experimental data than does the BIT modeling with source terms.

#### ACKNOWLEDGEMENTS

The authors are grateful for the financial support of the National Natural Science Foundation of China (11502097), the Natural and Science Foundation of Jiangsu Province (BK20130478), the Foundation of Senior Talent of Jiangsu University (2015JDG158), and the China Postdoctoral Science Foundation (2016M591781). Our special thanks are due to Dr. Feng's Group for assistance with the experiments and valuable discussions and to the anonymous reviewers for insightful suggestions on this work.

#### ELECTRONIC SUPPLEMENTARY MATERIAL

The online version of this article (doi:[10.1007/s11837-017-2327-5](https://doi.org/10.1007/s11837-017-2327-5)) contains supplementary material, which is available to authorized users.

#### REFERENCES

1. Y.X. Liu and J. Li, *Modern Aluminum Electrolysis* (Beijing: Metallurgical Industry Press, 2008), pp. 3–8.
2. M.A. Cooksey, M.P. Taylor, and J.J.J. Chen, *JOM* 60, 51 (2008).
3. L.I. Kiss, A.L. Perron, S. Poncsak, and T.N. Guyen, *Light Metals 2007*, ed. M. Sørli (Orlando: TMS, 2007), pp. 495–500.
4. Y.Q. Feng, W. Yang, M.A. Cooksey, and M.P. Schwarz, *J. Comput. Multiph. Flows* 2, 179 (2010).
5. S.Q. Zhan, M. Li, J.M. Zhou, J.H. Yang, and Y.W. Zhou, *Light Metals 2014*, ed. J. Grandfield (San Diego: TMS, 2014), pp. 777–782.
6. R. Oey, R. Mudde, and H. Van den Akker, *AIChE J.* 49, 1621 (2003).
7. N.J. Zhou, X.X. Xia, F.Q. Wang, and J. Cent, *South Univ. T.* 14, 42 (2007).
8. J. Li, Y.J. Xu, H.L. Zhang, and Y.Q. Lai, *Int. J. Multiph. Flow* 37, 46 (2011).
9. Y.Q. Feng, M.P. Schwarz, W. Yang, and M.A. Cooksey, *Metall. Mater. Trans. B* 46, 1959 (2015).
10. M. Ishii and N. Zuber, *AIChE J.* 25, 843 (1979).
11. L.A. Schiller and Z. Nauman, *Ver. Dtsch. Ing.* 77, 135 (1935).
12. M.V. Tabib, S.A. Roy, and J.B. Joshi, *Chem. Eng. J.* 139, 589 (2008).
13. R. Rzehak and E. Krepper, *Int. J. Multiph. Flow* 55, 138 (2013).
14. Y. Sato, M. Sadatomi, and K. Sekoguchi, *Int. J. Multiph. Flow* 7, 167 (1981).
15. M.A. Cooksey and W. Yang, *Light Metals 2006*, ed. T.J. Galloway (San Antonio: TMS, 2006), pp. 359–365.
16. ANSYS Inc., *ANSYS Fluent 14.5 User's Guide* (Canonsburg: Fluent Inc., 2012).
17. S.Q. Zhan, M. Li, J.M. Zhou, J.H. Yang, and Y.W. Zhou, *J. Cent. South Univ. T.* 22, 2482 (2015).
18. S.Q. Zhan, *Ph.D. Dissertation*, Central South University, Changsha, 2015.
19. C. Simonin and P.L. Viollet, *Int. J. Numer. Methods Fluids* 91, 65 (1990).
20. A.A. Troshko and Y.A. Hassan, *Int. J. Multiph. Flow* 27, 1965 (2001).